Met. Mater. Int., Vol. 19, No. 2 (2013), pp. 135~145
doi: 10.1007/s12540-013-2001-6

Precipitate Prediction Model of Mg-xAl(x=3,6,9) Alloys

Byeong Deok Lee, Eun Jeong Kim, Ui Hyun Baek, and Jeong Whan Han*

Division of Material Science and Engineering, Inha University, Incheon 402-751, Korea

(received date: 3 February 2012 / accepted date: 9 May 2012)

A model was developed to predict the precipitation of $Mg_{17}Al_{12}$ in Mg-(3,6,9)wt%Al alloys. The phase equilibrium of the Mg-Al alloy system was calculated in detail by utilizing a phase diagram calculation commercial package and other thermodynamic data for Mg alloys. The precipitation kinetics of Al in Mg-(3,6,9)wt%Al alloys after different thermal treatments were studied by measuring electrical resistivity and hardness. The results obtained were explained by a model based on a simple nucleation and growth model and were compared with the measured precipitates volume fraction. And, the experimental results agreed on the thermodynamic data with the conditions of 12 hr for Mg-3Al, 30 min for Mg-6Al, 15 min for Mg-9Al alloys. Therefore, the model was applied to predict the effects of the precipitation of $Mg_{17}Al_{12}$.

Key words: Mg alloys, electrical resistivity, precipitation, nucleation, coarsening

1. INTRODUCTION

Magnesium alloy has the lowest density among existing common alloys and is very important in lowering the weight of transportation vehicles, such as automobiles and airplanes [1,2]. Such magnesium alloys have been limited in their use due to their low ductility and corrosion resistance compared to other light materials, but with the advancement of the alloy and refining technology, many limitations have been overcome [3-6]. Recently, the automobile industry has become greatly interested in the applications of magnesium alloy. Automobile industries all around the world are developing low polluting and low mileage cars to respond to environmental restrictions. Therefore, many parts in automobiles are becoming lighter to reduce energy use [6-8] and to solve environmental issues with lighter cars. There are many materials that are being developed for various automobile parts with high strength and high tenacity, such as steering wheel cores and the seat frames [9-11].

A strengthening method for a high strength and highly moldable Mg alloy usually employs either strength or educing strength. Notably, the alloy technology that employs an educing method is actively being researched. Also, recently, thermodynamics and the speed theory model have been used to research the movements of the deposits, which are expected to contribute to future alloy development. Notably, deposition research is being actively carried out with Al and Fe alloys [12-14]; however, the deposition movement research that utilizes thermodynamics and the speed theory model with Mg alloys is lacking. The Mg-Al alloy is the most commonly used traditional alloy that exhibits a cellular transformation depending on the alloy structure and [15] the prescribing temperature, as elucidated by continuous research on the structural change characteristics as well as the nuclear production organizations, but the studies on its deposit movements are still insufficient.

To improve the mechanical properties, magnesium alloys had precipitates distributed in their matrix and precipitate grain control technology was also used. If you control the properties of magnesium, these studies will easily contribute to the design of new alloys. Also, these alloys will contribute useful information of new Mg alloys to industries that utilize Mg through an appropriate combination of information, such as structure, type, proportion, shape, and distribution of precipitates. But, thermodynamic data for the development of a thermodynamic and kinetics model of precipitate behavior in Mg alloys have not yet been obtained. Therefore, it is essential to obtain all the data regarding the design of Mg alloys. Also, prediction technology needed establishment by technology assessment for the thermodynamic behavior of the precipitate and kinetics model of the development through experimental and theoretical approaches with empirical verification the thermodynamic factors and precipitate. Study of the predicted size and distribution of precipitate by thermodynamic and kinetic models was very complicated due to the difficulty of considering deposition rates, diffusion coefficients, and interfacial energy. Therefore, in this study, the reviewed theoretical definition of the behavior of precipitates in alloying elements and heat treatment processes and

*Corresponding author: jwhan@inha.ac.kr

precipitation/dispersion was to obtain data on the quantitative control as basic study of Mg-(3,6,9)wt% Al alloys accurate size and distribution prediction of precipitate. Finally, thermodynamic data was calculated to calculate the precipitate fraction that was need to predict the size and distribution of precipitation by a commercial program.

2. EXPERIMENTAL AND THEORETICAL METHODS

2.1. Experimental procedure

We used the KJMA [15] equation to calculate the volume fraction of the $Mg_{17}Al_{12}$ Phase with respect to aging time. To calculate the volume fraction of precipitates, it will find parameter values, such as nucleation rate and growth rate. Parameter values used to calculate volume fractions of precipitates are shown in Table 3. Also, the chemical potential energy and Gibbs energy, as they vary with temperature, were calculated by using a commercial program(Pandat). Before we calculated the volume fraction of the precipitates, the calculation results of each phase diagram and precipitate phase for the Mg-(3,6,9)wt%Al alloys were necessary to be determined in order to be applied as basic data.

The thermodynamic data of the parameters needed for accurate precipitation fraction calculations were converted to functions by the C-language. The data was inputted into the program. Quantitative data of the precipitate was calculated for heat treatment temperatures with times. The change of the precipitation amount was taken through microstructure analysis, resistivity, and hardness measurements. The data was compared with the results of experimental and theoretical calculations.

To compare the experimental results to the thermodynamic calculation results, the Mg-(3,6,9 wt%)Al alloys were prepared using high purity Mg and Al. A high purity Mg ingot (99.99 wt%) was melted in a graphite crucible heated from 700 to 730 ˚C and, after it was completely molten, an Al ingot with a purity of 99.99wt% was added to the melt. The crucible was then air cooled to room temperature. All the above procedures were conducted in a flowing protective gas (SF_6+CO_2) to prevent burning and oxidation. The specimen bars were prepared as rods (30 mmΦ×250 mmL). To observe the changes of the precipitate behavior of $Mg_{17}Al_{12}$, a solution heat treatment was performed for 24 h at 410 ˚C, and then aging was performed once per hour for up to 32 h at 170 ˚C to observe the aging characteristics. To observe the size and distribution of the precipitates, after the specimens were collected and mounted, SiC abrasive paper used to polish until #2000 and 0.05 μm alumina used to make mirror side. Etching was performed by optional corrosion with a chemical mixture (picric acid 6g+acetic acid 5 ml+distilled water 10 ml+ethyl alcohol 100 ml). The precipitate phase of $Mg_{17}Al_{12}$ was investigated with a scanning electron microscope (S-4300SE) and EDS.

After the solid solution treatment to investigate the continuous process of the phase transformation, the electrical resistivity specimens (15 mm×15 mm×0.8 mm) were prepared and 4-probe tests were performed. The aging temperature was maintained with an electricity furnace, under a constant DC power supply flow current (I) of 200 mA and a voltage drop (V) was calculated with an XY recorder. Therefore, the electrical resistance (R) could be obtained, and the electrical resistivity (ρ) was calculated by using the equation with measured area (A) and length (L). The electrical resistivity was in the following:

$$\rho = R\frac{A}{L} = \frac{V}{I}\times\frac{A}{L} \quad (1)$$

To compare with the precipitation behavior obtained by electrical resistivity, hardness was measured. The specimens with a size of 15 mm×15 mm×0.8 mm were subjected to isothermal heat treatments, and then a Rockwell Hardness Tester (SRH- DM) was used to measure the hardness with a load of 60 kg and a 1/16 inch steel ball. The hardness was measured by Rockwell hardness (HB) tester; the data were converted to HV units. The HB was measured at a minimum of ten points in order to reduce error. The variation of the precipitation fraction with aging time was analyzed using the microstructure method in the ASTEM E 1245 standard. The specimens (16 mm×10 mm) aged were observed with optical microscopy, as shown in Fig. 1.

2.2. Thermodynamic and kinetic model

The progress of the precipitates can generally be itemized into three concurring mechanisms: nucleation, growth, and coarsening. The main idea of this theory is that coarsening or Ostwald ripening results from the interaction of particles embedded within a matrix phase (α-Mg), whereby larger particles grow at the expense of smaller ones. Coarsening

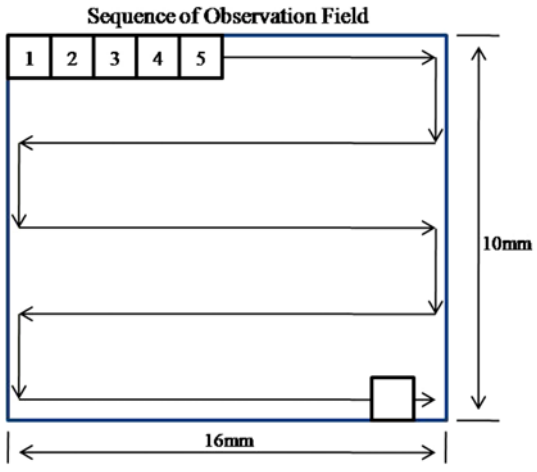

Fig. 1. Sequence of metallographic measurement.

takes place without remarkable change in the relative proportion of the two phases, which are possibly close to the equilibrium value predicted by the phase diagram. Given a conventional precipitate structure, smaller particles preferentially dissolve and transfer their mass to larger particles, which preferentially grow. The driving force for coarsening in a two-phase system is the lowering of the total interfacial energy and hence the total interfacial area. Therefore, larger individual particles are eventually produced in the matrix. In this study, the Lifshitz-Slyozov-Wagner (LSW) theory [16] predicts the rate of coarsening in alloys. These methods are employed in the description of diffusion processes of impurities and defects as well as solid-solid phase transformations.

2.2.1. Experimental rate equations

Goler et al. [18] formulated nucleation and growth rate equations for isothermal transformations. They assumed that the nucleation rate is constant, but collision between the particles was not considered. Therefore, the calculated results coincide with the results of experimental data at the initial time, but a large difference manifests as the reaction continues. The collision between two growing particles is considered by Johnson, Mehl, and Avrami [19,20]. They introduced the 'extended volume' concept, which considers collisions between growing particles by probabilistic relationships according to their actual transformation volume and expansion volume. Here, extended volume means a continuously grown volume without collisions of particles that are created at the transformation temperature. Thus, the 'extended volume' has great value when compared with the volume of the actual transformation. Avrami considered variation of the nucleation rate assuming heterogeneous nucleation. In other words, Avrami assumed nuclear generation at the faces, edges, and corners of grain boundaries and each nucleation position is exhausted as the transformation proceeds. Figure 2 shows nucleation rate against time and the formula is as follows:

$$\gamma = 1 - \exp(-kt^n) \tag{2}$$

where, γ is volume fraction, n is reaction quotient, k is rate constant, and t is time. The physical interpretation of the Avrami constants, k and n, is difficult and open to interpretation. Originally, n was held to have an integer value between 1 and 4 which reflected the nature of the transformation in question. In the derivation above, for example, the value of 4 can be said to have contributions from three dimensions of growth and one representing a constant nucleation rate. Alternative derivations exist where n has a different value [20]. If the nuclei are preformed, and so are present from the beginning, the transformation is only due to the 3-dimensional growth of the nuclei and n has a value of 3. An interesting condition occurs when nucleation occurs on specific

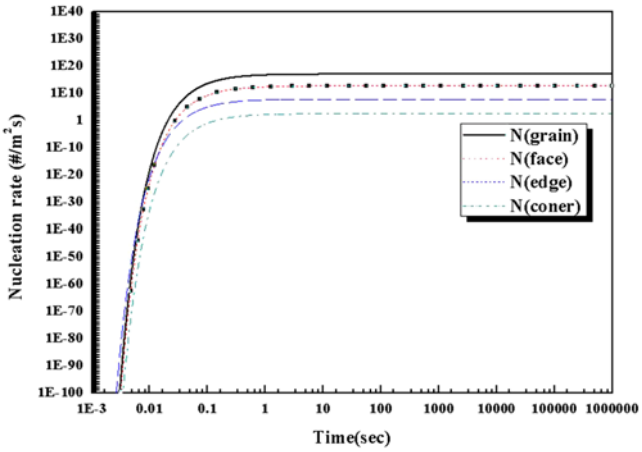

Fig. 2. Nucleation rate(#/m^{2}s) for site of Mg-9Al alloy.

sites (such as grain boundaries or impurities) which rapidly saturate soon after the transformation begins. Initially, nucleation may be random and growth unhindered, leading to high values of n (3, 4). Once the nucleation sites are consumed, the formation of new particles will cease. Furthermore, if the distribution of nucleation sites is non-random, then the growth may be restricted to 1 or 2-dimensions. Site saturation may lead to n values of 1, 2, or 3 for surface, edge, and point sites, respectively [21].

2.2.2. Classical nucleation rate model

Nucleation rate theory of the solid-state has been redefined by Aaronson [22]. Their theory is not suitable for accurate quantitative analysis without using accurate thermodynamics and kinetics data, but it can be used in qualitative analysis to compare the relative importance of nucleation factors. For solid transformation in the steady state, the time-dependent nucleation rate (J) with diffusion control indicates the following.

$$J = N_v Z\beta^* exp\left(-\frac{\Delta G}{k_b T}\right) exp\left(-\frac{\tau}{t}\right) \tag{3}$$

where N_v: is Nucleation site density (#/m^2), Z: is Zeldovich factor, β^*: is frequency factor for atomic mobility of precipitate in matrix, τ: is incubation time [sec], t: is time [sec], k_b: is Boltzman constant [J K^{-1}], V: is Growth rate [m/s] of precipitate, ΔG^*: is Gibbs free energy [J K^{-1}], γ^*: is Critical nucleus radius [m], D: is diffusivity of solute, C: is concentration, and X: is mole fraction of solute.

$$N_v = \left(\frac{\lambda}{d}\right)^{3-M}\left(\frac{N_0}{V}\right) \tag{4}$$

$$Z = \frac{V_m \Delta G_V^2}{8\pi(kTK\gamma^3)^{\frac{1}{2}}} \tag{5}$$

$$\beta^* = \frac{16\pi\gamma^2 DXL}{a^4 \Delta G_V^2} \quad (6)$$

$$\tau = \frac{12kTa^2\gamma}{DX(V_m)^2(\Delta G_V)^2} \quad (7)$$

$$V = \frac{D}{r^*}\left(\frac{C_M}{C_{p/M}} - \frac{C_{M/P}}{C_{M/P}}\right) \quad (8)$$

$$\Delta G^* = \frac{16\pi\gamma^3}{3(\Delta G_V - \Delta G_S)^2} \quad (9)$$

$$r^* = \frac{2\gamma}{(\Delta G_V - \Delta G_S)} \quad (10)$$

In the solid phase, when precipitate nucleates constantly, the J of the time-dependent nucleation rate is linearly proportional to the Zeldovich factor, frequency factor, nucleation site density, etc., but it is exponentially proportional to the nucleation free Energy barrier, ΔG^* and the incubation period for nucleation, τ. Therefore, the dominant factors of the time-dependent nucleation rate J can be considered to be ΔG^* and τ. By calculating ΔG^* and τ, the precipitation behavior will be able to be understood when homogeneous nucleation occurs.

3. RESULTS AND DISCUSSION

3.1. Thermodynamic calculations for precipitates of Mg-(3,6,9)wt%Al alloys.

3.1.1. General observations and equilibrium calculations

The calculated phase diagrams of the Mg-Al alloys (calculated with thermodynamic calculations (see Fig. 3(a))) and precipitate/distribution phase analysis progressed as follows. We investigated the analysis of thermodynamic calculation data for the phase diagrams and precipitate phases of Mg-(3, 6,9)wt%Al alloys. In the case of the Mg-9Al alloy, the maximum solubility of Al was 12.7 wt% at 437 ℃. We confirmed that the β-$Mg_{17}Al_{12}$ phase existed during the solidification process. Also, the phase volume and change of the precipitate start temperature during the cooling process were calculated and are shown in Fig. 3(b). During cooling, the steady state of the Mg-9wt%Al alloy appeared α-Mg while the alloys started melting at its liquidus temperature of 600 ℃. The precipitate start temperature of $Mg_{17}Al_{12}$ was approximately 359 ℃. In this study, the maximum volume fraction was about 0.16 at 170 ℃ and that was chosen as the heat treatment temperature. This basic data was effective for volume analysis of precipitates.

3.1.2. Volume fraction model from the KJMA equation

Volume fractions of precipitate for the Mg-(3,6,9,)wt%Al alloys were calculated by the KJMA (Kolmogolov-Johnson-Mehl-Avrami) equation [23].

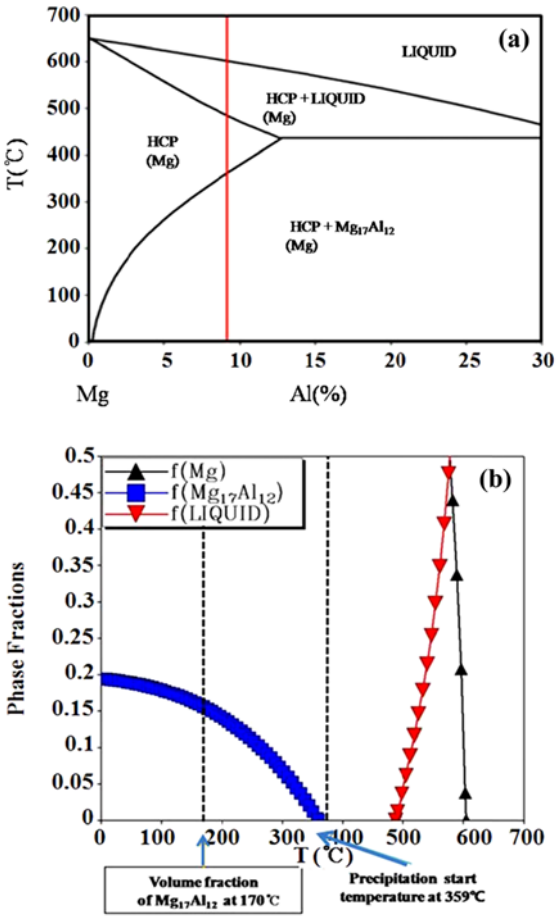

Fig. 3. Calculated phase diagram and phase fractions of Mg-9wt%Al.

$$f = 1 - \exp\left(-\int_0^t J(\tau)\cdot V(t,\tau)d\tau\right) \quad (11)$$

In order to obtain the Volume fraction (f), the nucleation rate data, J, and growth rate data, V, were required. After nucleation rate data and incubation period information were obtained, the nucleation rate was calculated by using the classical nucleation model (Eq. 4). Also, the parameters for calculating the nucleation rate were calculated by using equations (5)-(11).

3.1.3. Nucleation rate calculation

Parameters that include the chemical potential energy and Gibbs energy are important factors for calculating equations (5-11) needed for the nucleation rate calculation of Eq. (4). In this study, the chemical potential energy and Gibbs energy were calculated by a thermodynamics program. Interfacial energy, lattice parameter, and additional parameters for the calculation were obtained from the references in Table 3. First of all, the driving force calculation method of the

$Mg_{17}Al_{12}$ phase was instantiated for Mg-9Al. It is shown as follows:

$$\Delta G_v = G_n/V_m \tag{12}$$

$$\Delta G_n = \Delta G_2 - \Delta G_1 \tag{13}$$

$$G_1 = \mu_A^{\alpha} X_A^{\beta} + \mu_B^{\alpha} X_B^{\beta} \tag{14}$$

$$G_2 = \mu_A^{\beta} X_A^{\beta} + \mu_B^{\beta} X_B^{\beta} \tag{15}$$

where G_1 and G_2, are the Gibbs energy and were calculated by the thermodynamics program. The program can calculate the driving force (ΔG_n). ΔG_n can be calculated from the free energy from respective equilibrium states, compositions, and chemical potentials. This calculation result is shown in Table 1. But, for the process that formed a precipitate during the general heat treatment, it was not required for a long time to reach and maintain an equilibrium state. Therefore, this system does not correspond to equilibrium state data. In this study, kinetic factors which were used to calculate ΔG_n and predict the kind of precipitates from quasi-equilibriums were considered. Figure 3 shows how the G_2 and G_1 were used to calculate ΔG_n for $Mg_{17}Al_{12}$. And, Figure 4 shows calculated value of $Mg_{17}Al_{12}$ precipitate for the alloys. For the initial composition of a supersaturated solid solution, the chemical potential of that composition can be calculated by the calculated volume fracture. The composition of the precipitates could be predicted as a binary equilibrium calculation between the solid solution and the respective solution's precipitates. ΔG_n of the precipitates from the supersaturated embryo phase could be obtained from the calculated results and we consider the $Mg_{17}Al_{12}$ phase to be a precipitate phase during heat treatment. The ΔG_n of the $Mg_{17}Al_{12}$ phase for Mg-(3,6,9)wt%Al alloys at 359 °C was calculated by thermodynamic calculations and where "0" corresponds to ΔG_n, as shown in Fig. 4, ΔG_n increases as temperature decreases because, when supercooling is increasing, low temperatures act on the driving force of precipitation during the solidification of alloys. Also ΔG_v ($\Delta G_v = G_n/V_m$), which is necessary to calculate the activity energy (ΔG^*) from Eq. (10) was obtained by ΔG_n. The result calculated from ΔG_v, such as the resulting calculation of G_n, increased as the temperature decreased (supercooling causes growth) and the calculated result is about 4×10^6 J/m^2 at 170 °C. The results of ΔG_v and ΔG^* are shown in Fig. 5 and the critical particle size and incubation period were calculated from previous calculation results and were used to calculate critical particle sizes ($r^* = 2\gamma/(\Delta G_V - \Delta G_s)$) at specific growth rates ($V = D/r^*(C_M/C_{p/m} - C_{M/P}/C_{M/P})$) and are shown in Fig. 6. The nucleus radius in the Mg-9Al alloy among the calculated results can be ana-

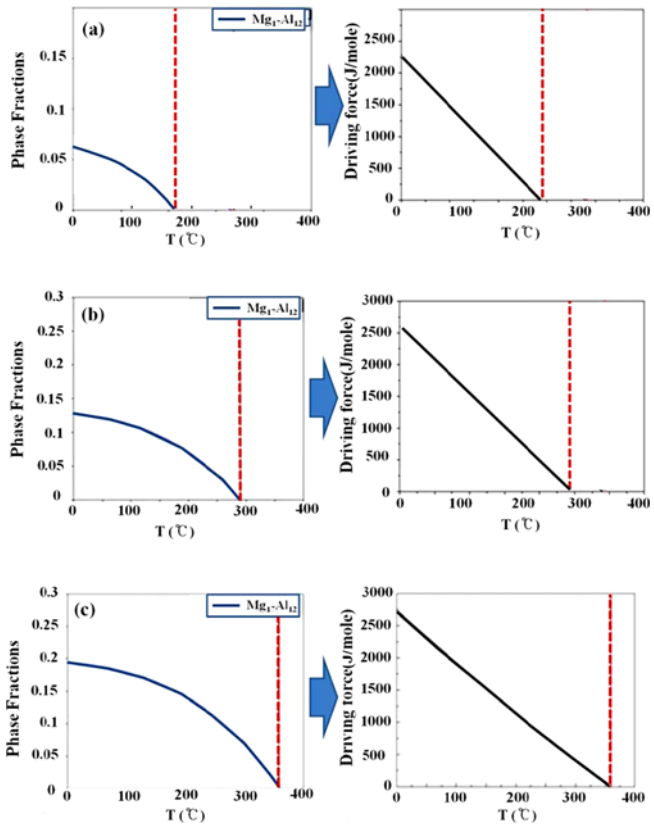

Fig. 4. Calculated driving force of (a) Mg-3Al (b) Mg-6Al and (c) Mg-9Al.

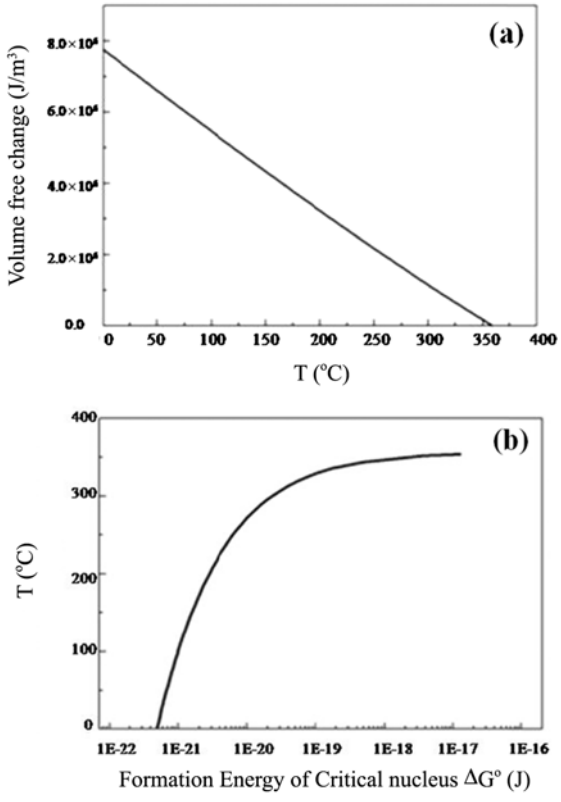

Fig. 5. Effect of temperature on (a) volume free energy change (ΔGv) and (b) activity energy change (ΔG*).

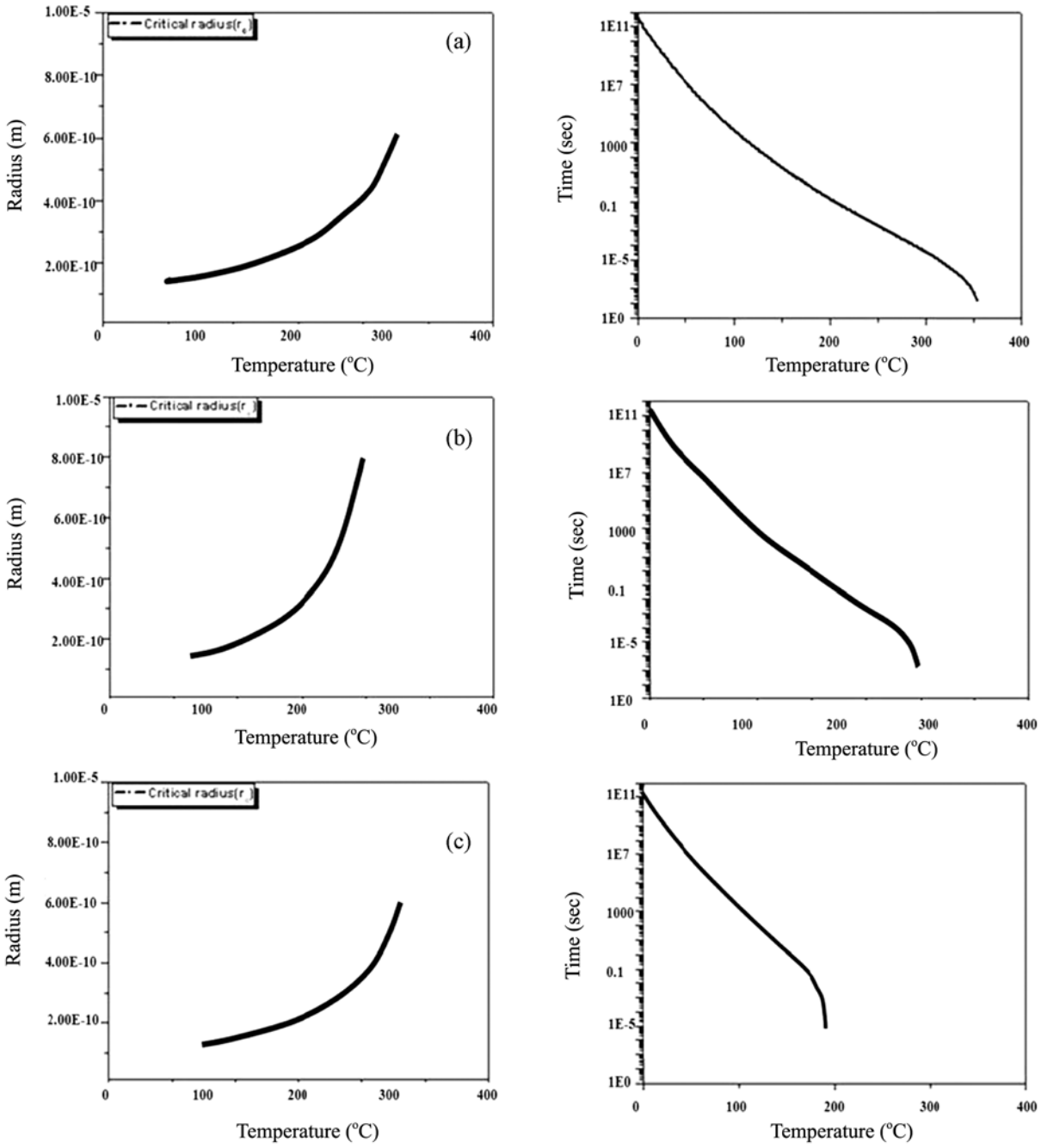

Fig. 6. According to alloy composition, critical nucleation radius (γ^*) and incubation period (τ): (a) Mg-3Al (b) Mg-6Al and (c) Mg-9Al.

lyzed as follows. At 300 °C, the critical particle size is about 7.5 nm, at 200 °C, it is about 2.4 nm, and at 100 °C, it is about 1.3 nm; this mean that the $Mg_{17}Al_{12}$ phase creates nucleation sites from embryos to particles. Increased supercooling causes ΔG_v to increase and the active energy to decrease. The reduction of the active energy is the means by which it is easy to create nucleation due to growth down the energy barrier. In addition, the critical radius was reduced, as according to the calculation results. Also, the incubation period calculation of Eq. (8) could be calculated by thermodynamic calculation data and the references from Table 3.

We used for diffusion coefficient reported by Moreau *et al*. [25] and the parameters that were used are shown in Table 3. The incubation period calculation results show that as the temperature decreases, the incubation period increases, and this is shown in Fig. 6. Also, the effect of the critical nucleus radius (γ^*), energy barrier, and incubation period for supercooling on creating nucleation was organized by the thermo-

Table 1. Thermodynamic properties of Mg-Al alloys from the thermodynamic program

T (℃)	μ (Aα) (J)	X (A)	μ (Bα) (J)	X (B)	G_2 (J)
Mg-9Al					
80	–11825.3	0.585962	–10735	0.414038	–13464.2
120	–13386.8	0.586018	–13014.7	0.413982	–15001.6
152	–14713	0.586212	–14914.3	0.413788	–16311
200	–16820.4	0.586873	–17880.5	0.413127	–18398.7
248	–19058.9	0.588129	–20976.7	0.411871	–20626
304	–21823	0.590521	–24740.7	0.409479	–23390.2
Mg-6Al					
80	–11346.8	0.414038	–11781.5	0.585962	–13464.2
120	–13333.8	0.586018	–13755.4	0.413982	–15001.6
152	–14652.5	0.586212	–15758.2	0.413788	–16311
200	–16748.8	0.586873	–18879.1	0.413127	–18398.7
248	–18976.2	0.588129	–22130	0.411871	–20626
Mg-3Al					
80	–12689	0.439595	–12689	0.439595	–13464.2
120	–13270.8	0.560463	–15321.3	0.439537	–15001.6
152	–14582.2	0.560659	–17503	0.439341	–16311

Table 2. Calculated parameter in Eqs. (8), (10), and (11)

T (℃)	γ^* (nm)	ΔG^* ($\times 10^{-21}$ J)	τ (sec)
Mg-3Al			
80	0.18	1.43	50538
120	0.29	3.6	136.56
153	0.56	13.2	1.228
Mg-6Al			
80	0.13	0.714	101559
120	0.16	1.11	442.479
153	0.2	1.74	9.2764
200	0.315	4.18	0.06810
248	0.69	20.1	4.8×10^{-4}
Mg-9Al			
80	0.11	0.567	127904
120	0.137	0.791	620
152	0.161	1.07	16.48
200	0.213	1.9	0.149
248	0.312	4.1	0.0023
304	0.65	17.8	2.16×10^{-5}

Table 3. Parameter of Mg-Al from the literature

Parameter of $Mg_{17}Al_{12}$	Value	Ref.
Interfacial energy ( )	0.01 J/m^3	[24]
Volume diffusion coefficient for Al (D_0)	$1.210^{-3}$$m^2$/s	[25]
Lattice parameter (a)	10.54 nm	[26]

dynamic calculation. Parameters in Table 1, 2, and 3 were deducted by from the calculated nucleation rate. This result was calculated by Eq. (4), as shown in Fig. 7. Figure 7(b) shows the variation of nucleation rates at 100, 120, and 150 ℃ for the sample of the calculation result for nucleation rate of Mg-9Al. As one can see in Fig. 7, we confirmed that the nucleation was finished, and in the case of an incubation

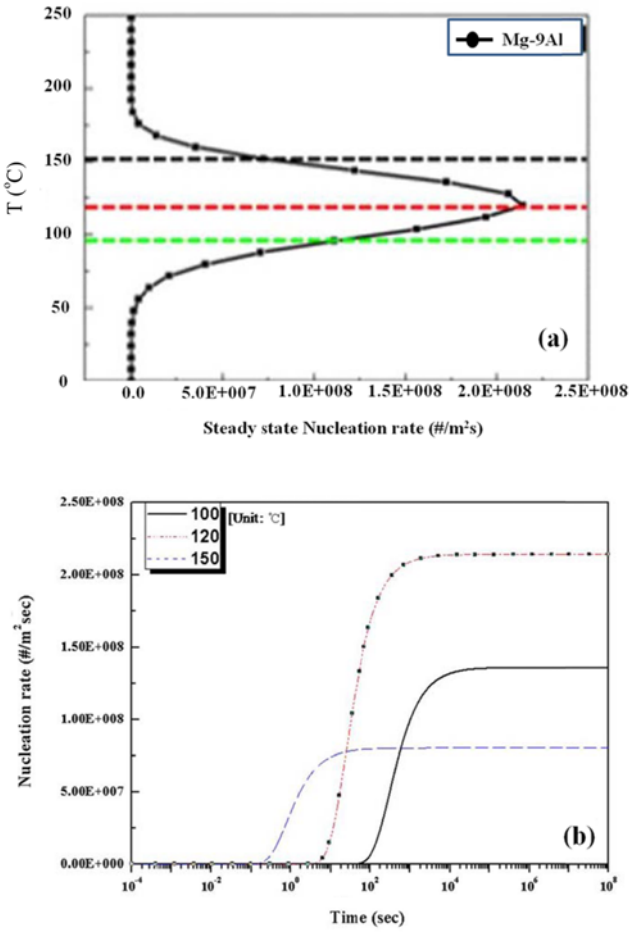

Fig. 7. Calculated nucleation rate of Mg-9Al alloys; (a) steady state nucleation rate (J*) according to temperature and (b) nucleation rate (J*) at 100, 120, and 150 ℃.

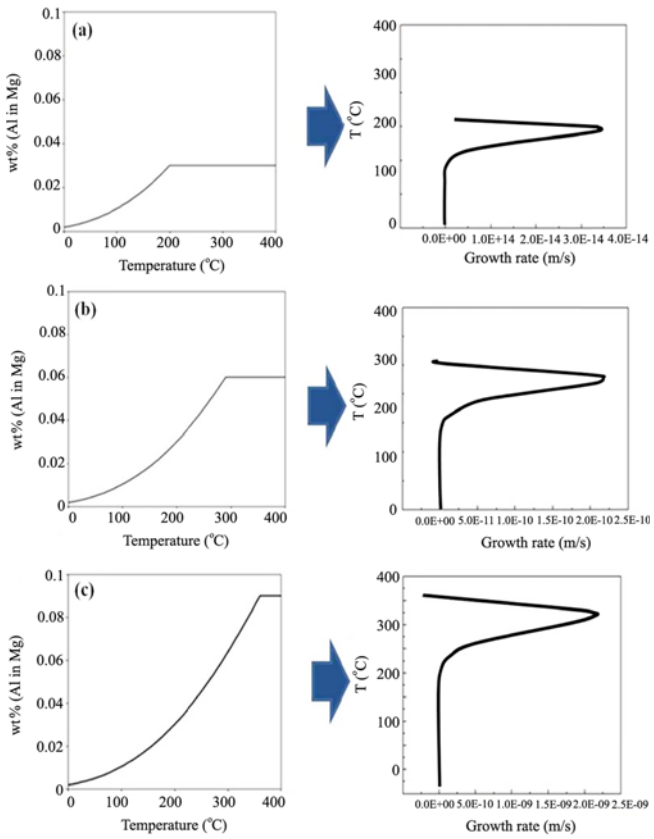

Fig. 8. Calculated growth rate (V) from equilibrium concentration of Al for (a) Mg-3Al (b) Mg-6Al and (c) Mg-9Al.

period of 150 °C, the completion time is 10 sec, whereas at 100 °C it is approximately 10^4 sec. Also when the maximum nucleation rate based on the temperature calculation is used to calculate the nucleation rate time, the nucleation was finished at 10^3 sec. In this case, the nucleation rate was about 210^8#/m^2s, and the nucleation rate was calculated for a maximum temperature of 120 °C.

3.1.4 Growth rate calculation

The growth of precipitates occurred after the nucleation of precipitates; the $Mg_{17}Al_{12}$ phase behavior could be explained by growth by spherical diffusion control of the Al solute atom in Mg. The growth rate of spherical particles was calculated by growth rate equations, and this is shown in Fig. 8. The calculation result indicates that as the temperature increases, the growth rate of the $Mg_{17}Al_{12}$ phase increases. This growth rate is decided by the diffusion of solute in the matrix and the concentration grade. And this can consider the effect of alloy composition and temperature. This result is explained by Fig. 9. At any time, the growth rate is proportional to the supersaturation. When supercooling is small, supersaturation becomes small. And, when supercooling is large, diffusion is slowed. As a result, the growth rate was slowed. So the maximum growth rate was expressed at the middle of supercooling. Separated the diffusion areas of $Mg_{17}Al_{12}$ phase was stacked. It was not applied to the growth rate equation. The growth rate rapidly decreased. When the embryo concentration becomes Xe at many different locations, the growth is stopped.

3.1.5. Volume fraction calculation of the $Mg_{17}Al_{12}$ phase

The kinetic volume fraction of the $Mg_{17}Al_{12}$ phase was calculated by using the KJMA equation with the calculated parameters. The calculation method, incubation period time, volume fraction and growth time were calculated for the isothermal state at 170 °C. After coding Gaussian integration law in visual basic, the calculated parameter calculated by Excel was applied to the volume fraction calculation and the input link function for high accuracy. The variation of the kinetic volume fraction for the Mg-x(3,6,9)wt.%Al alloys at an isothermal temperature of 170 °C is shown in Fig. 10. The incubation period of the Mg-3wt%Al alloys ranges from 12 h to 84 h. In the case of the Mg-6wt%Al alloys, the incubation period ranges from 1 h to 4 h. The volume fraction is 0.0856 for the equilibrium state. In the case of Mg-9wt%Al, the incubation period ranged from 40 min to 3 h. The volume fraction is 0.1554 for the equilibrium state. The kinetics of the incubation period and the quantitative data of the temperature were obtained by the calculation results of the respective alloys.

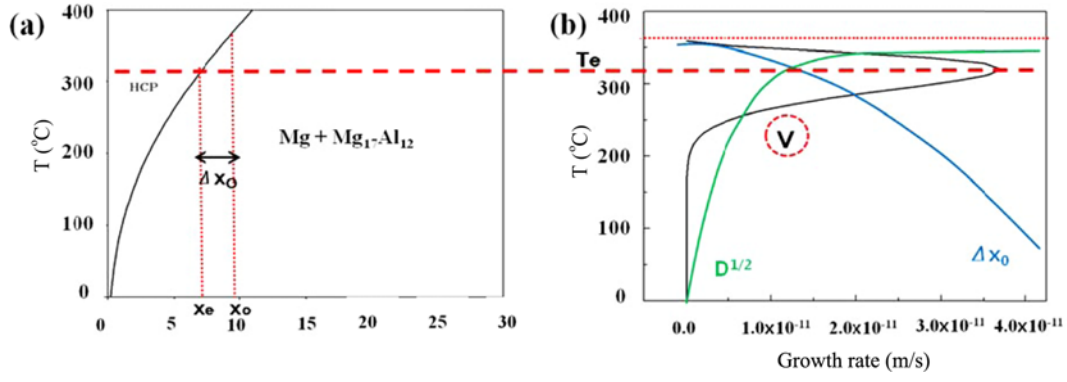

Fig. 9. Effect of temperature on (a) mole fraction of equilibrium phase and (b) variation of growth rate for Mg-9Al.

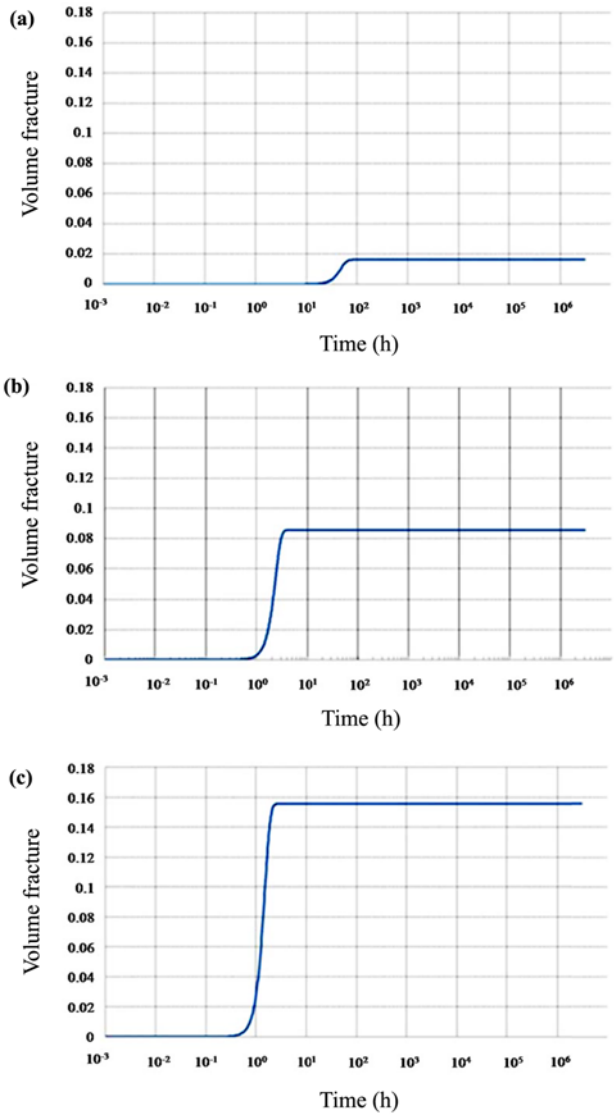

Fig. 10. Calculated volume fraction in the KJMA equation for (a) Mg-3Al, (b) Mg-6Al, and (c)Mg-9Al at 170 ℃.

3.2. Electrical resistivity with aging time at 170 ℃

Solution treatment of Mg-(3,6,9)wt%Al alloys was performed for 12 h at 410 ℃. The electrical resistivity changes of the Mg-(3,6,9)wt%Al alloy are shown in Fig. 11 for the period during the isothermal heat treatment at 170 ℃. As a result, the variation of resistivity can be represented by two stages. Because there are no Al precipitation phenomena, the first stage does not change the resistivity. With precipitates of the $Mg_{17}Al_{12}$ phase in the Mg matrix, stage 2 is the step of reducing the resistivity. Figure 11(a) shows the variation of resistivity for the Mg-3Al alloy during isothermal heat-treatment at 170 ℃.

The $Mg_{17}Al_{12}$ precipitate variation of the Mg-3Al alloy occurring in the range of resistivity values exhibited a decrease of its overall change and the thermodynamic calculations and resistivity experiments shown in the incubation period exhibited similar patterns. But, the precipitate fraction such as calculated results increases in the range of resistivity values that were observed to increase slightly; also, while the Mg-6Al and Mg-9Al precipitate time decreased, the $Mg_{17}Al_{12}$ precipitate for the Mg-3Al alloy required a lot of time [21]. Thus, we considered continuous measurement of the electrical resistance generating the oxide film in specimens connected to the Cu read. Figure 11(b) shows the variation of the specific resistance value during the aging time of the Mg-

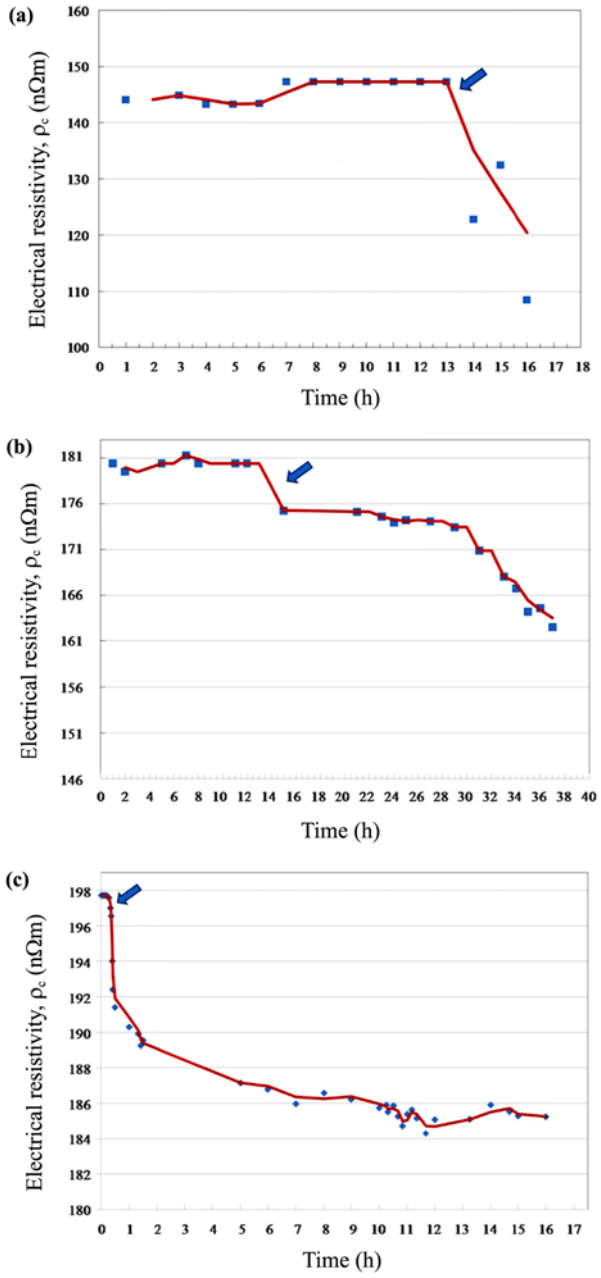

Fig. 11. Variation of the electrical resistivity with aging time at 170 ℃ for (a) Mg-3Al (b) Mg-6Al (c) Mg-9Al.

6Al alloy. The Mg-6Al experimental conditions were with the same as the experimental methods of the Mg-3Al alloy. The specimens were connected with the Cu lead, and set up to a constant-current of 200 mA.

During the aging time of the Mg-6Al alloys, the resistivity values were reduced after about 1hr. The incubation period of the experimental results and thermodynamic calculations show a similar pattern, and the change of resistivity is considered to be due to the precipitation behavior of the $Mg_{17}Al_{12}$ phase. In the study, we consider that the variation of resistivity with aging time can be associated with the precipitate behavior of the $Mg_{17}Al_{12}$ phase. Figure 11(c) shows the variation of the specific resistance value during the aging time of the Mg-9Al alloy. The resistivity value of the specimen aged for about 15 min did not change significantly. However, the resistivity value decreased after being aged for about 1 h. And, the resistivity value continuously decreased from this point. As a result, we consider the variation of resistivity with aging time can be associated with the precipitate behavior of the $Mg_{17}Al_{12}$ phase. And, the incubation period of the experimental results and thermodynamic calculations for the Mg-9Al alloy exhibit similar patterns. This is the same as the previous study on the Mg-(3,6)wt%Al alloy. In this study, the improvement of thermal electrical conductivity results in decreased resistivity values based on the electrical resistance analysis. In order to understand the experimental methods, our experimental results were compared with thermodynamic calculations, such as incubation period and precipitate time. We can see that the experiment results are analogous to thermodynamic calculations, as shown in Figs. 10 and 11.

3.3. Variation of hardness with aging time at 170 °C

Figure 12 shows the hardness variation with aging time at 170 °C. With an aging time of 32 h, the maximum hardness of the Mg-3Al alloy and Mg-6Al alloys were about 49 Hv and 51 Hv, respectively. With on aging time of 8 h, the maximum hardness of the Mg-9 alloy was about 58 Hv. So, the hardness increases with the concentration of Al and the time to reach maximum hardness value was found to decrease. In the study, we can see that, with an increase of the solid solubility of Al in the α-Mg phase, the hardness increased in the Mg-(3,6,9,)wt%Al alloys with an aging time of 170 °C. Precipitates in the Mg-9Al alloy were generated within approximately 15 min. And, the growth of the precipitates increased the hardness. In addition, we consider that the Mg-6Al alloys in the growth time range of about 30 min as well as the Mg-3Al alloys in the growth time range of about 12 h increased in hardness by generating precipitates. Clark [27] reported that the transformation completion degree can be seen through the hardness analysis. And, the analysis accuracy in the initial precipitate stage of the hardness analysis was higher than the microstructure analysis. In the study, it is

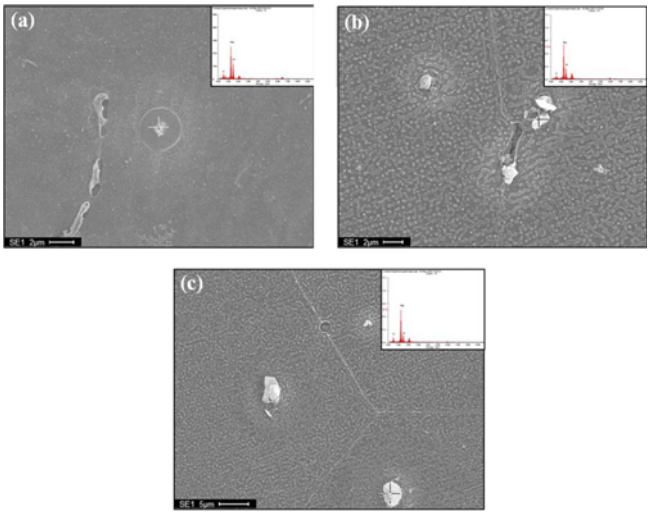

Fig. 13. SEM micrograph and EDS analysis of (a) Mg-3Al aged at 170 °C for 12 h, (b) Mg-6Al aged at 170 °C for 1 h, and (c) Mg-9Al aged at 170 °C for 30 min.

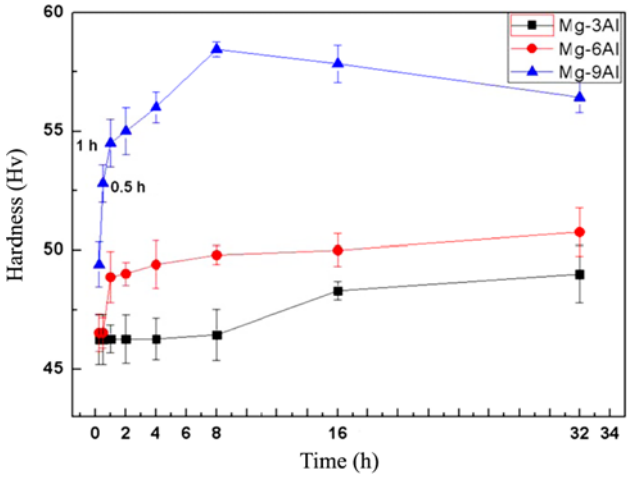

Fig. 12. Variation of the hardness value of heat-treated specimens with aging time. Mg-3Al, Mg-6Al, and Mg-9Al.

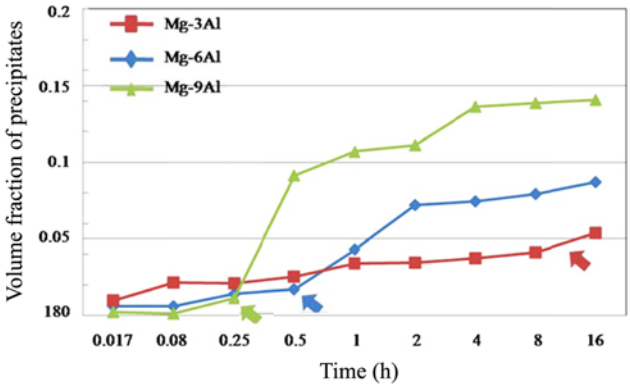

Fig. 14. Variation of the volume fraction of precipitate with aging time for Mg-3Al, Mg-6Al, and Mg-9Al.

consistent to compare hardness analysis to the thermodynamic calculation and resistivity analysis.

3.4. Image analysis of precipitates

Figure 13 shows the precipitate phase of the Mg-(3,6, 9)wt% Al alloys aged for 12 h, 1 h, and 30 min as they were observed by SEM/EDS analysis. And, we can see that the distribution of the $Mg_{17}Al_{12}$ phase is at the grain boundary and is trans-granular in the α-Mg matrix. To compare the thermodynamic calculations and the experimental analysis of the precipitate fractions, specimens aged for the each time were prepared according to ASTEM E 1245. Then, the microstructure image was calculated by an image analysis program (IMGE PRO PLUS) using the counting method; the calculated results are shown in Fig. 14. Precipitate fraction variation of the Mg-3Al alloy was observed to increase after aging treatment for 8 h. Precipitate fraction variation of the Mg-6Al alloy appeared after about 30 min. Lastly, the precipitate fraction variation of the Mg-6Al alloy began after about 15 min, which is faster than the alloys of the other compositions. As a result, we suggest that the precipitate phase could be related to hardness and because the analyzed results have similar values, precipitates of the $Mg_{17}Al_{12}$ affect the elevation of hardness values. In addition, the results of the previous thermodynamic calculations, resistivity, and hardness analyses indicate similar tendencies.

4. CONCLUSIONS

We prepared the classical model of nucleation and growth rates for Mg alloys' precipitate behaviors based on the development of kinetic modeling. Regarding the quantitative data of the precipitates, our results include the nucleation rate, incubation period, and growth rate calculated by using a thermodynamic calculation program. Next, the prepared parameters were characterized through Excel and a Gaussian-integration-coding to visual basic program. We also show the analysis of the incubation period and maximum precipitate rate related to hardness, image, and electric resistivity measurements for the reliability of the precipitation rate.

The experimental results agreed on the thermodynamic data with the conditions of 12 h for Mg-3Al, 30 min for Mg-6Al, 15 min for Mg-9Al alloys. Therefore, it is assumed that the precipitation rate could increase according to increments of the hardness value. Finally, our results demonstrated of the calculation of the precipitate rate of the Mg-Al alloys and these could be useful for basic data on the calculation of other individual particle phases.

ACKNOWLEDGMENTS

This work was supported by a grant from Inha University for author's research of 2012.

REFERENCES

1. S. Zhou, L. Liu, J. P. Jung, M. Y. Lee, and Y. Norman Zhou, *Met. Mater. Int.* **16**, 967 (2010).
2. B. D. Lee, U. H. Baek, K. S. Jang, H. T. Son, and J. W. Han, *Korean J. Met. Mater.* **49**, 440 (2011).
3. B. H. Lee, S. M. Kim, M. E. Mehtedi, E. Evangelista, and C. S. Lee, *Met. Mater. Int.* **6**, 197 (2010).
4. D. B. Lee, T. D. Nguyen, and Y. J. Kim, *Met. Mater. Int*. **16**, 761 (2010) .
5. B. D. Lee, U. H. Baek, and J. W. Han, *J. Mater. Eng. Performance*, DOI: 10.1007/s11665-011-0111-1 (2012).
6. D. H. Kim, H. K. Lim, Y. K. Kim, J. S. Kyeong, W. T. Kim, and D. H. Kim, *Met. Mater. Int*. **17**, 383 (2011).
7. K. S. Song, H. C. Jung, and K. S. Shin, *Met. Mater. Int.* **17**, 397 (2011).
8. S. Y. Chang, D. H. Lee, B. S. Kim, T. S. Kim, Y. S. Song, S. H. Kim, and C. B. Lee, *Met. Mater. Int.* **15**, 759 (2009).
9. C. Antion, P. Donnadieu, F. Perrard, A. Deschamps, C. Tassin, and A. Pisch, *Acta Mater.* **51**, 5335 (2003).
10. D. H. Ping, K. Hono, and J. F. Nie, *Scripta Mater.* **48**, 1017 (2003).
11. J. E. Park, H. R. Kim, S. H. Ahn, and Y. W. Chang, *Met. Mater. Int*. **15**, 515 (2009).
12. S. H. Lee and K. J. Lee, *J. Kor. Inst. Met. & Mater*. **45**, 389 (2007).
13. S. Banerjee, P. S. Robi, and A. Srinivasan, *Met. Mater. Int*. **16**, 523 (2010).
14. J. H. Park, I. H. Jung, and S. B. Lee, *Met. Mater. Int*. **15**, 677 (2009).
15. J. H. Kim, F. Barlat, C. M. Kim, and K. S. Chung, *Met. Mater. Int*. **15**, 125 (2009).
16. C. D. Lee and C. S. Kang, *J. Kor. Met. & Mater*. **39**, 71 (2001).
17. B. Niethammer and R. L. Pego, *SIAM J. Math. Anal.* **31**, 467 (2000).
18. V. Goler, F. Sachs, and G. Sachs, *Z. Phys*. **77**, 281 (1932).
19. W. A. Johnson and R. F. Mehl, *Trans. AIME* **135**, 416 (1939).
20. M. Avrami, *J. Chem. Phys*. **7**, 1103 (1939).
21. A. K. Jena and M. C. Charturvedi, *Phase Transformation in Materials*, p.111, Prentice-Hall, Englewood Cliffs, NJ (1992).
22. J. W. Cahn, *Acta Metallurgica*, **4**, 572 (1956).
23. A. N. Kolmorgorov, A statistical theory for the recrystallization of metals, No. 3, p.355, IZv, Akad. Nauk. SSSR., Ser. Matem (1937).
24. C. R. Hutchinson, J. F. Nie, and S. Gorsse, *Metall. Mater. Trans. A* **36**, 2093 (2005)
25. G. Moreau, J. A. Cornet, and D. Calais, *J. Nucl. Mater.* **38**, 197 (1971).
26. Schobinger-Papamantellos et al., *Die Naturwissenschaften.* **57**, 128 (1970).
27. J. B. Clark, *Acta metall*. **16**, 141 (1968).